A Micro-Silicon Chip for *in Vivo* Cerebral Imprint in Monkey

Affif Zaccaria,*[,†] Ali Bouamrani,[‡] Laurent Selek,[†,▽] Michelle El Atifi,[†] Anne Marie Hesse,[§] Aurélie Juhem,[⊥] David Ratel,[‡] Herve Mathieu,[#] Yohann Coute,[§] Christophe Bruley,[§] Jerome Garin,[§] Alim L Benabid,[‡] Stephan Chabardes,[∥,▽] Brigitte Piallat,[∥] and François Berger[†,‡]

[†]Institut des Neurosciences Team 7 Brain Nanomedicine, INSERM U836, UJF, CHU, Grenoble, France

[‡]Clinatec, CEA-LETI, Grenoble, France

[§]Biologie à Grande Echelle, IRTSV, CEA, Grenoble, France, and INSERM, U1038, Grenoble, France.

[⊥]Ecrins therapeutics, BIOPOLIS, 38700 La Tronche, France

[∥]Institut des Neurosciences Team 11 Brain Function and Modulation, INSERM U836, UJF, CHU, Grenoble, France

[▽]Department of Neurosurgery, Centre Hospitalier Universitaire, Grenoble, France

[#]Institut des Neurosciences Team 5 Functional and Metabolic Neuroimaging, INSERM U836, UJF, CHU, Grenoble, France

Ⓢ *Supporting Information*

ABSTRACT: Access to cerebral tissue is essential to better understand the molecular mechanisms associated with neurodegenerative diseases. In this study, we present, for the first time, a new tool designed to obtain molecular and cellular cerebral imprints in the striatum of anesthetized monkeys. The imprint is obtained during a spatially controlled interaction of a chemically modified micro-silicon chip with the brain tissue. Scanning electron and immunofluorescence microscopies showed homogeneous capture of cerebral tissue. Nano-liquid chromatography−tandem mass spectrometry (nano-LC-MS/ MS) analysis of proteins harvested on the chip allowed the identification of 1158 different species of proteins. The gene expression profiles of mRNA extracted from the imprint tool showed great similarity to those obtained via the gold standard approach, which is based on post-mortem sections of the same nucleus. Functional analysis of the harvested molecules confirmed the spatially controlled capture of striatal proteins implicated in dopaminergic regulation. Finally, the behavioral monitoring and histological results establish the safety of obtaining repeated cerebral imprints in striatal regions. These results demonstrate the ability of our imprint tool to explore the molecular content of deep brain regions *in vivo*. They open the way to the molecular exploration of brain in animal models of neurological diseases and will provide complementary information to current data mainly restricted to post-mortem samples.

KEYWORDS: Neurodegenerative diseases, cerebral imprints, in vivo, tissue harvesting, proteomics, transcriptomics
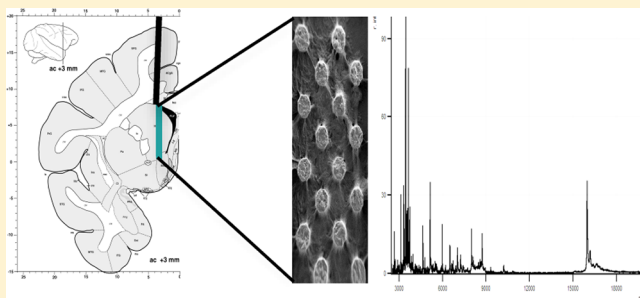
With the demographic aging and the augmentation of the life expectancy, age-related neurodegenerative disorders are an increasing public health problem. Until now, the exact pathogenetic mechanisms underlying the degenerative process in neurological diseases are still not understood.[1] In fact, the relative inaccessibility of cerebral tissue impedes the molecular analysis of pathological brain regions in the early postdiagnostic stage. Although genomic expression studies[2−5] or proteomic analyses[6−8] of human cerebral tissues permit correlation of some biological pathways, including mitochondrial and proteasomal dysfunctions or oxidative stress, to neurological diseases, all of these results have been restricted to post-mortem samples and are generally derived during advanced disease stages. With the development of animal models of neurodegenerative diseases in primates,[9] accessibility to and analysis of the brain at different stages of degeneration is now conceivable.[10] However, this requires the sacrifice of the animal, rendering impossible brain molecular follow-up in the same

animal.[11] In fact, performing several biopsies in the same brain regions is unthinkable because of the lesion effects caused by current biopsy tools.[12] We recently developed a new tool specifically adapted for brain tissue imprints. The harvesting surface is based on a silicon chip, which harbors chemical and structural modifications. During a surgical approach less traumatic than biopsy, we demonstrated that this microchemically modified surface, when exposed to the specific investigated brain area, provides local cellular capture. As a result of anionic capture, both cells and extracellular matrices are harvested providing a unique opportunity for *in situ*, spatially oriented bioharvesting. On the basis of this concept, we have developed a specific device for primate research. In this study, we assessed

(i) the capacity of our tool to harvest brain molecules in the putamen and caudate nucleus (i.e., striatum) of a healthy monkey and (ii) the lesional effects induced by repeated targeting in basal ganglia. Molecular investigations on the tissue captured by the silicon chip demonstrated the compatibility of our strategy with large-scale transcriptomic and proteomic studies. Furthermore, the behavioral monitoring of the animals following repeated brain tissue imprints did not reveal any obvious modification. Finally, both the postmortem imaging and histological analyses confirmed the minimal lesion-effect induced by our tool.

■ RESULTS AND DISCUSSION

In this study, we present a new tool developed by our group and designed to obtain cerebral imprints in the basal ganglia of monkeys (Figure 1). This tool is based on a silicon chip, which
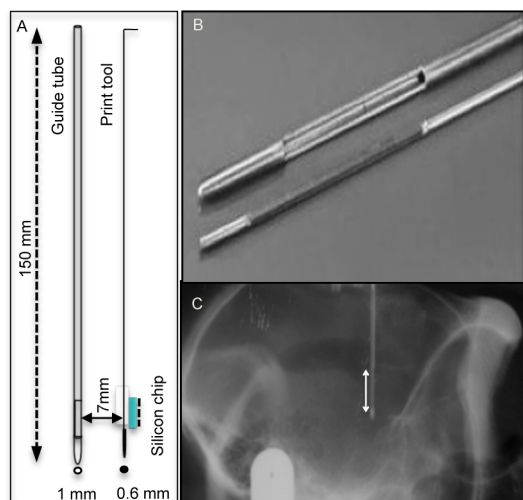
Figure 1. Tool design and X-ray scan of a cerebral imprint (A) Schematic representation of the imprint tool. The guide tube prevents the capture of nonspecific tissue during the descent. The exposure of the silicon chip by a 180° rotation of the inner tool allows harvesting of the desired tissue. (B) Picture of the imprint tool. (C) X-ray scan of the monkey skull during the execution of a cerebral imprint in the caudate nucleus. The window of exposure (white arrow) is easily seen.

has been chemically and structurally modified. To prevent the capture of tissue in nonspecific regions, the silicon chip is hidden during the insertion and removal of the tool. Once the tool is inserted into the targeted region, the silicon chip is exposed via the window of the guide tube, allowing the tissue imprint to be obtained. The main aims of this study were to confirm (i) the capacity to perform multimolecular analysis from *in vivo* cerebral imprints and (ii) the safety of repeated cerebral imprints in the basal ganglia. Five different cerebral imprints were performed at different times in both caudate nucleus and putamen of two different monkeys. We performed 10 different cerebral imprints in two monkeys, and only 8 imprints have been displayed in this study.

After each cerebral imprint, motor and finger-skill tests were performed to monitor potential behavior modifications of each monkey. Baseline assessment of the distances moved (Figure 2A) and the velocities of movement (Figure 2B) were significantly different between the two monkeys (Mann–Whitney test; distance moved, p value = 0.0089; velocity, p value = 0.0091). However, for each monkey, repeated cerebral

imprints in the putamen and caudate nucleus had no significant effect on the distances moved and the velocities of movement, compared with their individual baseline values (Mann–Whitney test; p value > 0.05). From the first to the fifth imprint, behavior assessments were not progressively worsened, confirming there is no cumulative effect induced by repeated tool insertion (Figure 2C). The same results were obtained with finger-skill tests (Figure 2D); the time required to pick up rewards in three different wells was significantly different between the two monkeys at baseline (p value = 0.0002), while for each monkey, no difference was observed before and after cerebral imprints ($p < 0.05$). These results suggest that our tool may allow repeated cerebral imprints in basal ganglia without functional lesion-induced effects.

To confirm the *in vivo* capture of tissue on the silicon chip, we performed scanning electron micrography (SEM). As shown in Figure 3A, the cerebral imprint permitted homogeneous capture of a thin layer of putamen tissue on the silicon chip (left picture). A focus on the micropillar surface showed the presence of a variety of cells (middle), including elongated and adherent cells with extensive processes (right). To identify the cell subtypes captured on the chip, immunofluorescence labeling was performed using antibodies against GFAP and NeuN. As shown in Figure 3A, apart from blood contamination, putamen tissue fixed on the chip was identified as neurons (NeuN positive nuclei) and astrocytes (GFAP positive cells). These results demonstrate the ability of the tool to harvest a homogeneous, thin layer of brain tissue. Thus, a spatial cellular fingerprint is obtained providing a unique tridimensional spatially oriented biocapture.

To further characterize the molecular content of the freshly harvested tissue, we used nano-liquid chromatography–tandem mass spectrometry (nano-LC-MS/MS) to identify the captured proteins.

We first quantified the total protein amount present on the chip. Four different cerebral imprints performed in putamen and caudate nucleus of both monkeys revealed an average capture of 16.3 ± 4.8 μg of proteins. The qualitative capture of different proteins by the chip was assessed by both MS profiling and 1D sodium dodecyl sulfate–polyacrylamide gel electrophoresis (SDS–PAGE) migration (Figure 4A). Both techniques revealed the harvesting of many different mass proteins despite the presence of hemoglobin around 15 kDa. In addition to these approaches, we performed an extensive proteomic characterization of the tissue harvested on the chip. The amount of recovered material, approximately 16 μg of total proteins, permitted analysis of the sample by nano-LC-MS/MS and a total of 1158 different proteins were identified and considered for further analysis.

The presence of brain associated proteins such as glial fibrillary acidic protein (GFAP), neuronal specific septin 3, synapsin 1, or neural cell adhesion molecules 1 and 2 (NCAM 1/2) confirmed the harvesting of cerebral parenchyma. The submission of these 1158 different species to Ingenuity Pathway Analysis[13] for functional characterization highlighted 347 and 91 different proteins, which have been described as implicated in neurological and psychological disorders, respectively (Figure 4C). These proteins are significantly implicated in brain specific signaling pathways such as axonal guidance and synaptic long-term potentiation or depression but also in neurological disease associated pathways such as Huntington or Parkinson's diseases (Table 1).
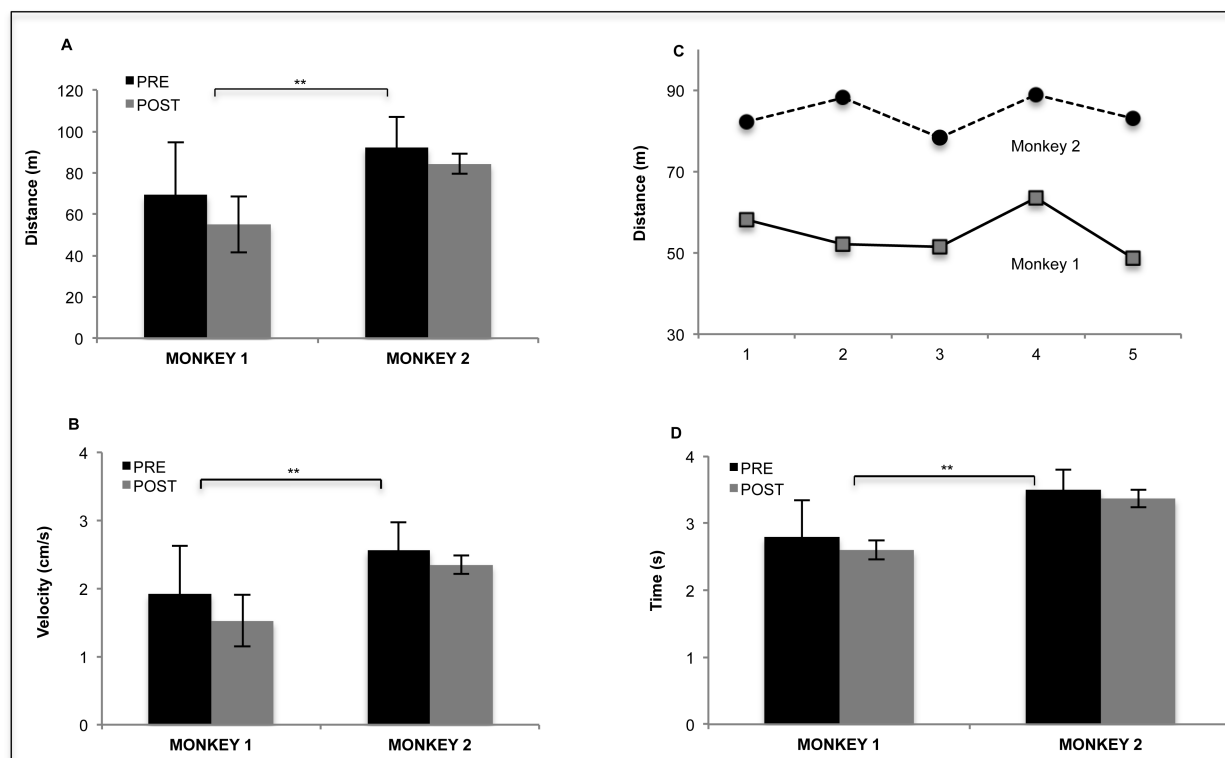
Figure 2. Motor activities of monkeys after repeated cerebral imprints. Distance moved (A) and velocity of movement (B). Animals were assessed by the video system for 60 min before the first cerebral imprint (PRE, $n = 5$) and after each imprint (POST, $n = 5$). Evolution of the distance moved after each cerebral imprint ($n = 5$) for both monkeys (C). Finger skill tests (D). Animals were assessed by the time required to pick up three peanuts in 1 cm wells before the first (PRE, $n = 15$) and after each cerebral imprint (POST, $n = 15$). Data are presented as the means $\pm$ SD ** $p < 0.01$, *** $p < 0.001$, Mann−Whitney test.
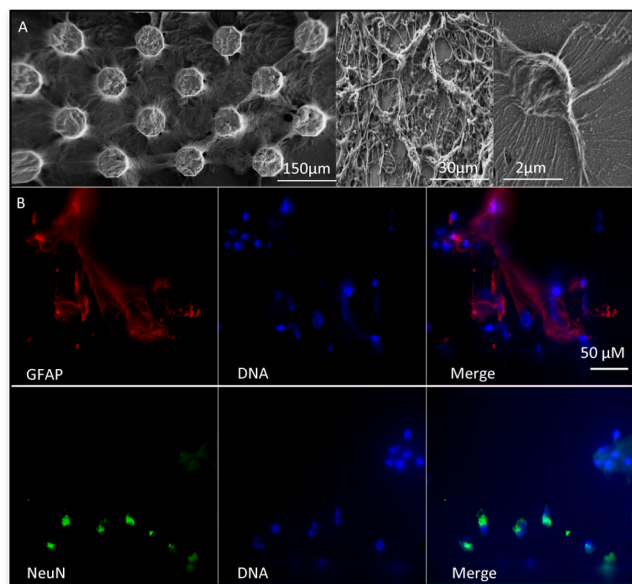
Figure 3. Microscopic observation of a cerebral imprint (A) Scanning electron micrograph showing (left) the homogeneous capture of tissue on the silicon chip, (middle) a variety of cells on the micropillar, and (right) an elongated cell with extensive processes. (B) Immunostaining of glial fibrillary acid protein (GFAP) and neuronal nuclei (NeuN) on the captured cerebral imprint. Astrocytes were identified as GFAP-positive and NeuN-negative cells (top) and neurons showed NeuN-positive nuclei without GFAP labeling (bottom). The chip was stained for GFAP (red), NeuN (green), and Hoechst (blue).
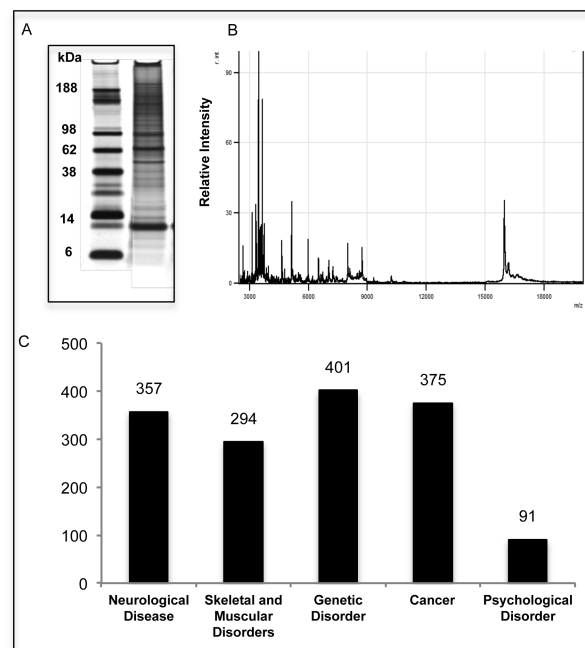
Figure 4. Proteomic analysis of the cerebral imprint. Analysis of proteins extracted from a cerebral imprint by 1D SDS-PAGE (A) and mass spectrometry profiling (B). (C) Functional annotation of the cerebral imprint proteome identified by nano-LC-MS/MS. The bar graph represents the number of identified proteins in each disease or disorder signaling pathways classified as the most significant using the Ingenuity Pathway Analysis software.

Table 1. Functional Analysis by Ingenuity Pathway Analysis[a]

Ingenuity canonical pathways	p-value	IPA DataBase	cerebral imprint	ratio (%)
Parkinson's signaling	1.00×10^{-3}	18	5	27.8
Huntington's disease signaling	3.16×10^{-14}	238	40	16.8
glioma invasiveness signaling	9.77×10^{-4}	60	9	15.0
synaptic long-term potentiation	1.74×10^{-5}	114	16	14.0
dopamine receptor signaling	$\mathbf{3.39 \times 10^{-5}}$	**95**	**13**	**13.7**
amyotrophic lateral sclerosis signaling	9.12×10^{-6}	119	16	13.4
glutamate receptor signaling	$\mathbf{9.77 \times 10^{-4}}$	**69**	**9**	**13.0**
axonal guidance signaling	2.00×10^{-14}	433	56	12.9
dopamine−DARPP32 feedback in cAMP signaling	$\mathbf{3.24 \times 10^{-3}}$	**187**	**16**	**8.6**
synaptic long-term depression	1.29×10^{-2}	147	12	8.1

[a]Signaling pathways significantly represented by the identified proteins from a putamen-targeted cerebral imprint. Pathways displayed in bold are associated with Parkinson's disease and putamen signaling. The ratio is calculated as the number of proteins from the cerebral imprint that map to the pathway divided by the total number of proteins described as associated with the pathway (IPA DataBase).

Moreover, the identification of α-synuclein,[14] DJ-1,[15] UCHL-1,[16] monoamine oxidase B,[17] superoxide dismutase,[18,19] and tyrosine hydroxylase[20] indicates that the cerebral expression of relevant proteins for PD studies could be determined by our approach in a living monkey. Finally, the identification of tyrosine hydroxylase and the significant expression of both dopamine receptor signaling and dopamine−DARPP32 feedback in cAMP signaling with IPA strongly suggest that the cerebral imprint had been performed in a brain region with dopaminergic activity, such as the putamen or caudate nucleus.[21−24] These results demonstrate the capacity of our tool to harvest and identify relevant proteins in specific brain regions.

Complementary to proteomics studies, microarray analysis provides considerable information about molecular pathways deregulated in neurodegenerative diseases,[25,26] particularly in PD.[27−29] This technology measures the mRNA levels of all known genes coding for proteins in a given sample simultaneously.[30] Because RNA is labile and subject to rapid degradation, extraction and quality control are critical to ensure a relevant analysis.[31] In general, microarray analyses are performed from post-mortem extracted RNA; here, we analyzed expression levels of RNA extracted from the caudate nucleus of a living primate. Two cerebral imprints were successively performed in the same caudate nucleus, and total RNA was extracted. We aimed to compare their similarity with RNA extracted from post-mortem sections of the same caudate nucleus, which is the gold standard method, used here as control samples. First, quality was controlled; the quality of the RNA extracted from the imprint tool was satisfactory and similar to the post-mortem sample (rRNA 28S/18S ratio = 1.1). The analysis of the cerebral imprints revealed 27% detected probe sets in common (i.e., 14691 out of 54675) with 95% reproducibility between the two imprints (Figure 5A) and a high correlation (Figure 5B) between their expression in imprint 1 (y) and 2 (x) ($y = 1.0002x$; $r = 0.994$). The control sections showed a detection ratio of 28% and 85%
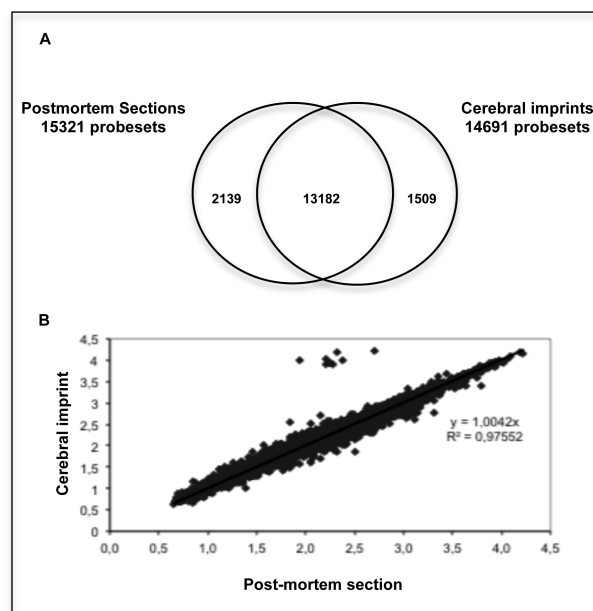

Figure 5. Assessment of RNAs from the cerebral imprint in comparison with RNAs from the corresponding post-mortem sections. (A) Venn diagram representing the extent of overlap of probe sets detected from RNA extracted from cerebral imprint and post-mortem sections. (B) Linear regression curve representing the intensity of expression of the common probe sets between cerebral imprints and post-mortem sections.

reproducibility between the two post-mortem sections (data not shown). The comparison of cerebral imprints and post-mortem sections revealed 89% detected probe sets in common (Figure 5A), and the linear regression curve (Figure 5B) revealed a great correlation between their expressions in imprints (y) and control samples (x) ($y = 1.0032x$; $r = 0.987$). These results revealed (i) the gene expression reproducibility of two consecutive cerebral imprints and (ii) similarity with gene expression of the gold standard post-mortem sections. Functionally, the capture by our tool of mRNA previously described by Bossers et al.[28] as differently expressed in a PD post-mortem caudate confirmed our ability to reach relevant transcriptomic information from our cerebral imprints.

The post-mortem MRI of one dissected brain confirmed the proper trajectories of our imprints (Figure 6B). GFAP staining was used to visualize astrocytes around the imprint tool tracks, because insertion of probes into the brain parenchyma induces a glial reaction. An increase in the density of glial cells and the length of glial cell processes is seen. Gliosis around imprint tool tracks was investigated using qualitative analysis at light and laser scanning microscopic levels of sections stained with the astroglial marker GFAP and the pan-microglia marker Iba-1. In the brain examined at 1 month after acute probe implantation, large, strongly stained "reactive astroglial cells" were observed around the probe tracks (Figure 6D). Increased GFAP staining up to 300 μm was observed at the imprint tool implantation site. In parallel, the Iba-1 staining was used to visualize microglia composition in the brain tissue around the tools acutely implanted with the imprint tool 1 month following implantation. We did not observe any microglia activation around the tracks; however, some macrophages were visualized in the tracks, possibly related to localized microbleeding (data not shown).
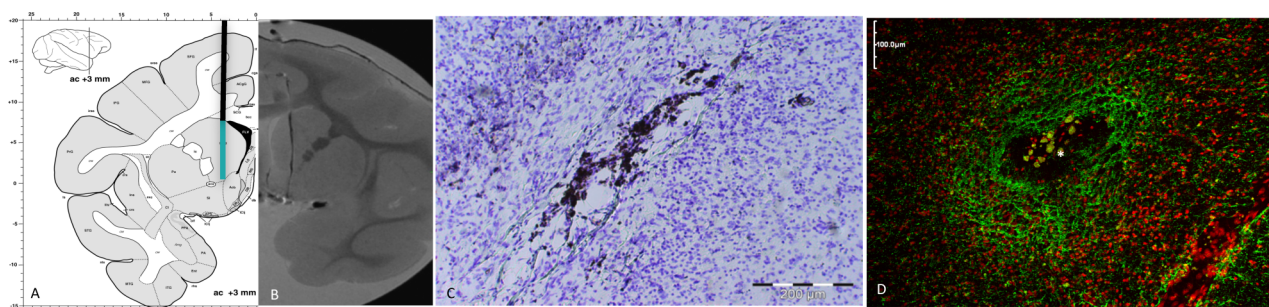
Figure 6. Brain tissue imprinting in monkey: A combined MRI and histological analysis. (A) A coronal plane of the Rhesus monkey brain atlas with the imprint tool trajectory. (B) Coronal MRI view of an imprint tool track in monkey caudate nucleus. (C) Photomicrograph showing cresyl violet staining around an imprint tool track. Calibration bar = 200 μm. (D) Photomicrograph showing astrocytes (GFAP staining, green) and counterstained cells (PI staining, red) around one imprint tool track (asterisk) following acute implantation in monkey caudate nucleus. Calibration bar = 100 μm.

CONCLUSIONS

The ability to access cerebral tissue is mandatory to better understand molecular mechanisms associated with neurodegeneration. The development of animal models such as the MPTP-monkey for PD provided the possibility to access brain tissue at different stages of neurodegeneration. However, the absence of an adapted tool for brain tissue harvesting limited studies to post-mortem samples.

This work introduces a new tool that could inform about *in vivo* molecular and cellular content of brain regions in monkey, through the harvesting of a thin layer of tissue. Repeated cerebral imprints in deep nucleus did not induce motor impairments and provided specific proteomic and transcriptomic information. In fact, one technical advance of this tool resides in its ability to expose the capture surface once in the targeted nucleus, preventing molecular contamination from other tissues. The capacity to perform several imprints on the same monkey at different times in different brain regions opens the way to a personalized molecular follow-up of brain. Different nuclei could be simultaneously or successively explored by proteomic or transcriptomic approaches to map the living brain and to complete information provided from post-mortem analyses. As classically observed after the introduction of microsurgical tools in the human brain, cerebral imprints also activated astrogliosis and induced microbleeding. We should be aware about the tissue damages induced by the tool introduction, which may affect protein and mRNA expression in targeted nuclei. In a context to understand molecular modifications induced by neurodegenerative diseases, imprint-induced modifications should be well characterized and distinguished from those induced by a pathological process through the use of unilateral model. Our approach could also be helpful in experiments assessing the molecular effects of strategies such as high-frequency stimulation[32] or gene therapy.[33]

MATERIAL AND METHODS

Animals. Experiments were conducted on two cynomolgus monkeys (*Macaca fascicularis*; CRP Port Louis, Mauritius): age 8 years old, weight 8 kg (monkey 1), and 10 years old, 11 kg (monkey 2). All experiments were carried out in accordance with the recommendations of the European Community Council Directives of 1986 (86/609/EEC), the National Institutes of Health Guide for the Care and Use of Laboratory Animals. The Ethics Committee of Region Rhône-Alpes approved the experimental protocol. Animals were kept with other congeners in an air-conditioned room under standard conditions of temperature (23 ± 1 °C), humidity (65% ± 4%), light (12 h light/dark cycle), and food/water available ad libitum.

Surgical Procedure. After induction under general anesthesia with ketamine−xylazine (10 mg−1 mg/kg, im, Imalgene, Centravet, France), the monkey's head was fixed in a Kopf stereotaxic frame (David Kopf Instruments, Tujunga, CA, USA). All operations were performed under sterile conditions. Ventriculography was performed by injecting a contrast medium into the anterior horn of the lateral ventricle at 27 mm anterior to the interaural line and 2 mm lateral to the midline with an angle of 20° anteroposteriorly. Positions of anterior (AC) and posterior (PC) commissures were identified on a sagittal radiograph. Cannulae were fixed on the skull bone above the right putamen at 3 mm posterior to AC and 11 mm lateral to the midline, and above the right caudate nucleus at 3 mm anterior to AC and 4.5 mm lateral to the midline, according to the stereotaxic atlas of *Macaca fascicularis* (BrainInfo, University of Washington, http://braininfo.rprc.washington.edu/). Analgesic/anti-inflammatory therapies (ketoprofen 2 mg/kg, im) and antibiotics (amoxicillin/clavulinic acid, 10 mg/kg, im) were administered during the postoperative period.

The Imprint Tool. The imprint tool is composed of three independent parts (Figure 1A,B). (1) A guide tube of 1-mm external diameter with a window of 7-mm. The length of the window has been chosen in accordance with the height of putamen and caudate nucleus at the coordinates of the cannula location. (2) A tool of 0.6-mm diameter with a dedicated space to support the silicon chip. (3) The silicon chip of 7-mm with an anionic surface and micropillar design to increase the interaction surface. Once inserted in the guide tube, rotation of the tool by 180° exposes or hides the chip in the window.

Behavioral Monitoring. To assess the potential lesions induced by brain imprints, cage activity levels were assessed in 1 h intervals (each Tuesday 10:00), before the first cerebral tissue imprint (control phase; n = 5) and 4 days after each imprint (n = 5). Behavioral measures, including distance traveled (m) and movement speed (cm/s) were quantified from videotape recordings using an automated video-tracking system, Ethovision (Noldus Information Technologies, The Netherlands).[34] The calibration of the software permitted determination of the position of the animal based on x and y coordinates, which were then used to calculate the different motor parameters.

At the end of each session, finger skill was also tested objectively by measuring the mean time required to pick up peanuts in three 1 cm diameter wells. The measure was included only if the monkey kept focus on the wells until all the peanuts had been collected. Mann−Whitney tests were performed using GraphPad InStat version 3.00 (GraphPad software, San Diego, California, USA).

Experimental Protocol. Every 15 days, under the same general anesthesia and sterile conditions, the monkey's head was fixed in a Kopf stereotaxic apparatus. The imprint tool was fixed to the stereotaxic manipulator. It was slowly inserted via the cannula so the window was exclusively in the putamen (i.e., 23 mm below the dura)

or the caudate nucleus (i.e., 20 mm below the dura). The silicon chip remained unexposed to the window during insertion of the cannula to prevent nonspecific molecular fixation. Once the cannula was inserted into the target, the tool supporting the silicon chip was rotated by 180° to expose the chip for 2 min, thus allowing the cerebral tissue to imprint. The chip was then hidden by a new rotation of the inner tool and the imprint tool was slowly removed from brain (Figure 1C). Overall, 10 tissue imprints (5 in each nucleus) were performed for both monkeys. Animals were sacrificed by sodium pentobarbital (150 mg/kg, iv) administration, and the brains were removed quickly after death. One brain was immediately frozen by immersion in isopentane (−45 °C) and then stored at −80 °C until molecular analysis. The other brain was immersion-fixed in 4% paraformaldehyde solution in 0.1 M phosphate buffer for 1 week and cryoprotected in 30% buffered sucrose until it sank. A post-mortem MRI was performed on the brain to confirm the trajectory of the cannulae. The brain was imaged in a Bruker Biospec USR AV III 4.7 T/400 mm scanner with a 600 mT/m field gradient interfaced with ParaVision 5.1 software (Bruker Biospec, Wissembourg, Germany). Images were acquired in the coronal plane.

Histology. The brain, after MR imaging, was then rinsed in 0.9% NaCl solution and frozen. Horizontal sections (50 μm) were collected from the imprint sites using a cryostat (Leica Microsystems, Nussloch GmbH). Some sections were processed to detect the implantation sites using cresyl violet staining. Antibodies used were raised against GFAP (rabbit polyclonal, diluted 1:1000, Dakocytomation, Glostrup, Denmark) as a marker for astrocytes, and Iba-1 (rabbit polyclonal, diluted 1:1000, Wako Chemicals GmbH, Neuss, Germany) was used as a pan-microglia marker. Incubations for primary antibodies were maintained overnight at 4 °C. After washing, the sections were incubated in Alexa 488 secondary antibodies (diluted 1:1000, Molecular Probes, Leiden, The Netherlands) for 1 h at room temperature. Counterstaining cells for confocal laser scanning microscopy was done with propidium iodide (Molecular Probes, Leiden, The Netherlands). After additional rinsing, the sections were mounted with Fluorsave (Merck KGaA, Darmstadt, Germany) and bound primary antibodies were visualized on a confocal microscope (Olympus, Hamburg, Germany).

Cerebral Imprint Microscopy. Two different chips from putamen were used for microscopy; one for scanning electron micrography and one for immunofluorescence.

Scanning electron micrography (SEM) was carried out to observe the distribution of the tissue harvested by the silicon chip. Immunofluorescence was used to confirm the presence of neurons and astrocytes on the chip in contact with putamen tissue.

To fix the tissue, the silicon chip was immersed into 1 mL of 4% PFA in PBS buffer for 30 min.

For SEM, the chip was then dehydrated through an ascending series of ethanol and critical point dried using CO_2. The chip was examined in an FEI Quanta 200 scanning electron microscope (FEI, Eindhoven, The Netherlands).

Immunofluorescence. After three washes in PBS, neurons and astrocytes were stained using NeuN (mouse antibody clone A60, Millipore) and GFAP antibodies (rabbit antibody, ab7260, abcam), respectively, diluted at 1:200 in PBST (PBS buffer and 0.5% Triton-X-100) for 1 h at RT. After three washes in PBST, the silicon chip was incubated with secondary polyclonal antibodies conjugated to Alexa 488 (anti-mouse) and Alexa 568 (anti-rabbit) (1:1000 dilution, Molecular Probes), and Hoechst 33258 at 2 μg/mL in PBST for 30 min at RT. After washes in PBST, the chip was mounted on glass slides and observed with a Zeiss Axiovert 200 M inverted microscope. Images were acquired using CoolSnap HQ (Photometrics) and a plan-apochromat 63× oil objective (Zeiss) with a black and white camera driven by the Metamorph software (Universal Imaging).

Proteomic Analysis. Two different cerebral imprints performed in putamen and two performed in caudate nucleus were used for proteomic analysis. Once the cerebral imprint was performed, the silicon chip was removed from the tool and rinsed 5 min in saline buffer to minimize blood contamination prior to protein extraction in 8 M urea buffer for 30 min under agitation. The total protein amount recovered from the tissue imprint was quantified by Bradford protein

assay (Bio-Rad Laboratories, Hercules, CA, USA). We performed MS profiling using cationic ProteinChip arrays (CM10, Biorad). The ProteinChips were equilibrated for 5 min with 150 μL of binding buffer (100 mM sodium acetate at pH 4). Two micrograms of total proteins was applied to each ProteinChip and incubated for 60 min at room temperature. The arrays were washed three times with the adequate binding buffer then rinsed with deionized water. After air-drying, 0.8 μL of saturated sinapinic acid matrix (50% acetonitrile, 0.5% trifluoroacetic acid) was added twice to each array spot. Profiling was performed on a MALDI mass spectrometer (Autoflex, Bruker) in a linear mode;. 5400 laser shots were acquired for each sample with a laser intensity of 55 and a matrix attenuation of 1000 Da. An extensive examination of the protein extract was also performed from one imprint by nano-LC-MS/MS. Fifteen micrograms of proteins was diluted in Laemli buffer and loaded in duplicate on SDS−PAGE gel (BioRad Laboratories) for protein electrophoresis migration. The gel was stained with Coomassie blue and sliced in 12 bands prior to iodoacetamide alkylation and in-gel digestion using trypsin. Peptides were extracted from gel bands and dried in a SpeedVac. Peptides were resuspended in 2% acetonitrile/0.2% formic acid buffer and injected into a nano-liquid chromatography system (Ultimate 3000, Dionex) coupled to an LTQ Orbitrap Velos (Thermo). Peptides were separated using a micro-precolumn cartridge (C18 Pepmap 100, LC Packings) and then separated using a 90 min RP gradient on a C18 column (Gemini C18 3 μm 100A, 75 μm × 150 mm).

Data were processed using Mascot server 2.3.0 (Matrix Science) using following parameters: Enzyme=Trypsin/P with a maximum of two missed cleavages, a mass tolerance of 10 ppm for MS and 1 Da for MS/MS, with a fixed modifixation of carbamidomethyl (C), and two variable modifications of acetyl (protein N-term) and oxidation (M). Validation and false-positive rate assessment were performed using IRMA and hEIDI softwares. Protein groups identified with a minimum of two different peptides were validated.

Our data set was further submitted to Ingenuity Pathway Analysis software (Ingenuity Systems, Redwood City, CA) to perform the functional characterization of the proteins recovered from the imprint tool. This automatic annotation tool uses a knowledge database and assigns proteins to functional classes or specific canonical pathways (CP) related to various biological processes.[13]

Transcriptomic Analysis. Two different cerebral imprints from the same caudate nucleus were used for transcriptomic comparison. Once the cerebral imprint was performed, the silicon chip was removed and quickly immersed in 500 μL of the lysis buffer from the mirVana isolation kit (Ambion, Applied Biosystems, Foster City, CA). Then, total RNAs were extracted from the cerebral imprint using the mirVana isolation kit, and their concentration was determined with the measure of absorbance at 260 nm. Their quality and RNA integrity were controlled by capillary electrophoresis migration using RNA Nano 6000 kit and the Bioanalyzer 2100 (Agilent Technologies, Palo Alto, CA). For microarray analysis, 200 ng of total RNA were amplified with the GeneChip 3′ IVT Express Kit. First, total RNA was reverse-transcribed using primers polydT-T7 promoter sequence; cDNA was double-stranded synthesized and finally amplified with biotinylated dNTP by the T7 RNA polymerase. Microarrays experiments were carried out in accordance with the protocol GeneChip Expression Wash, Stain and Scan from Affymetrix. Briefly, 15 μg of labeled cRNA was hybridized for 16 h at 45 °C on GeneChip Human Genome U133 Plus 2.0 (Affymetrix) corresponding to 54675 unique gene probe sets. The arrays were washed and stained with streptavidin−phycoerythrin before scanning. The fluorescence values of each probe set signal, reported in arbitrary units, were processed with MAS5 statistical algorithm to validate the probe set signal "absent" or " present", and finally they were normalized between all the arrays using the Robust Multichip Analysis (RMA) algorithm. These algorithms are included in Affymetrix expression console.

ASSOCIATED CONTENT

ⓢ Supporting Information

A complete list of all proteins identified. This material is available free of charge via the Internet at http://pubs.acs.org.

AUTHOR INFORMATION

Corresponding Author

*Mailing address: Grenoble Institut des Neurosciences, INSERM U836, Batiment Edmond J. Safra, Université Joseph Fourier, 38042 Grenoble cedex 9, France. E-mail: zaccaria. affif@gmail.com. Phone number: +33 (0)4 56 52 06 43.

Author Contributions

A.Z. designed and performed experiments, analyzed data, and wrote the paper. A.B. designed proteomic experiments and wrote the paper. L.S. performed experiments on animals. M.E.A. performed transcriptomic analysis. A.M.H., Y.C., C.B., and J.G. performed proteomic analysis. A.J. performed microscopy and wrote the paper. H.M. performed post-mortem MRI. D.R. performed histology and wrote the paper. A.L.B. contibuted to the study design. S.C. performed surgical procedures and supervised *in vivo* experiments. B.P. supervised and performed *in vivo* experiments. F.B. supervised the study and wrote the paper.

Notes

The authors declare no competing financial interest.

REFERENCES

(1) Moore, D. J., West, A. B., Dawson, V. L., and Dawson, T. M. (2005) Molecular pathophysiology of Parkinson's disease. *Annu. Rev. Neurosci. 28*, 57−87.

(2) Duke, D. C., Moran, L. B., Kalaitzakis, M. E., Deprez, M., Dexter, D. T., Pearce, R. K., and Graeber, M. B. (2006) Transcriptome analysis reveals link between proteasomal and mitochondrial pathways in Parkinson's disease. *Neurogenetics 7*, 139−148.

(3) Moran, L. B., Duke, D. C., Deprez, M., Dexter, D. T., Pearce, R. K., and Graeber, M. B. (2006) Whole genome expression profiling of the medial and lateral substantia nigra in Parkinson's disease. *Neurogenetics 7*, 1−11.

(4) Simunovic, F., Yi, M., Wang, Y., Macey, L., Brown, L. T., Krichevsky, A. M., Andersen, S. L., Stephens, R. M., Benes, F. M., and Sonntag, K. C. (2009) Gene expression profiling of substantia nigra dopamine neurons: Further insights into Parkinson's disease pathology. *Brain 132*, 1795−1809.

(5) Mandel, S., Grunblatt, E., Riederer, P., Amariglio, N., Jacob-Hirsch, J., Rechavi, G., and Youdim, M. B. (2005) Gene expression profiling of sporadic Parkinson's disease substantia nigra pars compacta reveals impairment of ubiquitin-proteasome subunits, SKP1A, aldehyde dehydrogenase, and chaperone HSC-70. *Ann. N.Y. Acad. Sci. 1053*, 356−375.

(6) Basso, M., Giraudo, S., Corpillo, D., Bergamasco, B., Lopiano, L., and Fasano, M. (2004) Proteome analysis of human substantia nigra in Parkinson's disease. *Proteomics 4*, 3943−3952.

(7) Kitsou, E., Pan, S., Zhang, J., Shi, M., Zabeti, A., Dickson, D. W., Albin, R., Gearing, M., Kashima, D. T., Wang, Y., Beyer, R. P., Zhou, Y., Pan, C., and Caudle, W. M. (2008) Identification of proteins in human substantia nigra. *Proteomics: Clin. Appl. 2*, 776−782.

(8) Licker, V., Cote, M., Lobrinus, J. A., Rodrigo, N., Kovari, E., Hochstrasser, D. F., Turck, N., Sanchez, J. C., and Burkhard, P. R. (2012) Proteomic profiling of the substantia nigra demonstrates CNDP2 overexpression in Parkinson's disease. *J. Proteomics 75*, 4656−4667.

(9) Emborg, M. E. (2007) Nonhuman primate models of Parkinson's disease. *ILAR J. 48*, 339−355.

(10) Bezard, E., Imbert, C., Deloire, X., Bioulac, B., and Gross, C. E. (1997) A chronic MPTP model reproducing the slow evolution of Parkinson's disease: evolution of motor symptoms in the monkey. *Brain Res. 766*, 107−112.

(11) Bezard, E., Dovero, S., Prunier, C., Ravenscroft, P., Chalon, S., Guilloteau, D., Crossman, A. R., Bioulac, B., Brotchie, J. M., and Gross, C. E. (2001) Relationship between the appearance of symptoms and the level of nigrostriatal degeneration in a progressive 1-methyl-4-phenyl-1,2,3,6-tetrahydropyridine-lesioned macaque model of Parkinson's disease. *J. Neurosci. 21*, 6853−6861.

(12) Bernstein, M., and Parrent, A. G. (1994) Complications of CT-guided stereotactic biopsy of intra-axial brain lesions. *J. Neurosurg. 81*, 165−168.

(13) Jimenez-Marin, A., Collado-Romero, M., Ramirez-Boo, M., Arce, C., and Garrido, J. J. (2009) Biological pathway analysis by ArrayUnlock and Ingenuity Pathway Analysis. *BMC Proc. 3* (Suppl 4), No. S6.

(14) Spillantini, M. G., Schmidt, M. L., Lee, V. M., Trojanowski, J. Q., Jakes, R., and Goedert, M. (1997) Alpha-synuclein in Lewy bodies. *Nature 388*, 839−840.

(15) Bonifati, V., Rizzu, P., van Baren, M. J., Schaap, O., Breedveld, G. J., Krieger, E., Dekker, M. C., Squitieri, F., Ibanez, P., Joosse, M., van Dongen, J. W., Vanacore, N., van Swieten, J. C., Brice, A., Meco, G., van Duijn, C. M., Oostra, B. A., and Heutink, P. (2003) Mutations in the DJ-1 gene associated with autosomal recessive early-onset parkinsonism. *Science 299*, 256−259.

(16) Maraganore, D. M., Lesnick, T. G., Elbaz, A., Chartier-Harlin, M. C., Gasser, T., Kruger, R., Hattori, N., Mellick, G. D., Quattrone, A., Satoh, J., Toda, T., Wang, J., Ioannidis, J. P., de Andrade, M., and Rocca, W. A. (2004) UCHL1 is a Parkinson's disease susceptibility gene. *Ann. Neurol. 55*, 512−521.

(17) Kurth, J. H., Kurth, M. C., Poduslo, S. E., and Schwankhaus, J. D. (1993) Association of a monoamine oxidase B allele with Parkinson's disease. *Ann. Neurol. 33*, 368−372.

(18) Marttila, R. J., Lorentz, H., and Rinne, U. K. (1988) Oxygen toxicity protecting enzymes in Parkinson's disease. Increase of superoxide dismutase-like activity in the substantia nigra and basal nucleus. *J. Neurol. Sci. 86*, 321−331.

(19) Saggu, H., Cooksey, J., Dexter, D., Wells, F. R., Lees, A., Jenner, P., and Marsden, C. D. (1989) A selective increase in particulate superoxide dismutase activity in parkinsonian substantia nigra. *J. Neurochem. 53*, 692−697.

(20) Javoy-Agid, F., Hirsch, E. C., Dumas, S., Duyckaerts, C., Mallet, J., and Agid, Y. (1990) Decreased tyrosine hydroxylase messenger RNA in the surviving dopamine neurons of the substantia nigra in Parkinson's disease: An in situ hybridization study. *Neuroscience 38*, 245−253.

(21) Graybiel, A. M. (1995) The basal ganglia. *Trends Neurosci. 18*, 60−62.

(22) Fienberg, A. A., Hiroi, N., Mermelstein, P. G., Song, W., Snyder, G. L., Nishi, A., Cheramy, A., O'Callaghan, J. P., Miller, D. B., Cole, D. G., Corbett, R., Haile, C. N., Cooper, D. C., Onn, S. P., Grace, A. A., Ouimet, C. C., White, F. J., Hyman, S. E., Surmeier, D. J., Girault, J., Nestler, E. J., and Greengard, P. (1998) DARPP-32: Regulator of the efficacy of dopaminergic neurotransmission. *Science 281*, 838−842.

(23) Greengard, P., Allen, P. B., and Nairn, A. C. (1999) Beyond the dopamine receptor: The DARPP-32/protein phosphatase-1 cascade. *Neuron 23*, 435−447.

(24) Hemmings, H. C., Jr., Nairn, A. C., Aswad, D. W., and Greengard, P. (1984) DARPP-32, a dopamine- and adenosine 3′:5′-monophosphate-regulated phosphoprotein enriched in dopamine-innervated brain regions. II. Purification and characterization of the phosphoprotein from bovine caudate nucleus. *J. Neurosci. 4*, 99−110.

(25) Hodges, A., Strand, A. D., Aragaki, A. K., Kuhn, A., Sengstag, T., Hughes, G., Elliston, L. A., Hartog, C., Goldstein, D. R., Thu, D., Hollingsworth, Z. R., Collin, F., Synek, B., Holmans, P. A., Young, A. B., Wexler, N. S., Delorenzi, M., Kooperberg, C., Augood, S. J., Faull, R. L., Olson, J. M., Jones, L., and Luthi-Carter, R. (2006) Regional and cellular gene expression changes in human Huntington's disease brain. *Hum. Mol. Genet. 15*, 965−977.

(26) Caudle, W. M., Bammler, T. K., Lin, Y., Pan, S., and Zhang, J. (2010) Using 'omics' to define pathogenesis and biomarkers of Parkinson's disease. *Expert Rev. Neurother. 10*, 925−942.

(27) Sutherland, G. T., Matigian, N. A., Chalk, A. M., Anderson, M. J., Silburn, P. A., Mackay-Sim, A., Wells, C. A., and Mellick, G. D. (2009) A cross-study transcriptional analysis of Parkinson's disease. *PLoS One 4*, No. e4955.

(28) Bossers, K., Meerhoff, G., Balesar, R., van Dongen, J. W., Kruse, C. G., Swaab, D. F., and Verhaagen, J. (2009) Analysis of gene expression in Parkinson's disease: Possible involvement of neuro-trophic support and axon guidance in dopaminergic cell death. *Brain Pathol. 19*, 91−107.

(29) Miller, R. M., Kiser, G. L., Kaysser-Kranich, T. M., Lockner, R. J., Palaniappan, C., and Federoff, H. J. (2006) Robust dysregulation of gene expression in substantia nigra and striatum in Parkinson's disease. *Neurobiol. Dis. 21*, 305−313.

(30) Geschwind, D. H. (2003) DNA microarrays: Translation of the genome from laboratory to clinic. *Lancet Neurol. 2*, 275−282.

(31) Imbeaud, S., Graudens, E., Boulanger, V., Barlet, X., Zaborski, P., Eveno, E., Mueller, O., Schroeder, A., and Auffray, C. (2005) Towards standardization of RNA quality assessment using user-independent classifiers of microcapillary electrophoresis traces. *Nucleic Acids Res. 33*, No. e56.

(32) Benabid, A. L. (2003) Deep brain stimulation for Parkinson's disease. *Curr. Opin. Neurobiol. 13*, 696−706.

(33) Kordower, J. H., Emborg, M. E., Bloch, J., Ma, S. Y., Chu, Y., Leventhal, L., McBride, J., Chen, E. Y., Palfi, S., Roitberg, B. Z., Brown, W. D., Holden, J. E., Pyzalski, R., Taylor, M. D., Carvey, P., Ling, Z., Trono, D., Hantraye, P., Deglon, N., and Aebischer, P. (2000) Neurodegeneration prevented by lentiviral vector delivery of GDNF in primate models of Parkinson's disease. *Science 290*, 767−773.

(34) Noldus, L. P., Spink, A. J., and Tegelenbosch, R. A. (2001) EthoVision: A versatile video tracking system for automation of behavioral experiments. *Behav. Res. Methods, Instrum., Comput. 33*, 398−414.